Journal of Nuclear Materials 376 (2008) 139–145

Contents lists available at ScienceDirect

Journal of Nuclear Materials

journal homepage: www.elsevier.com/locate/jnucmat

Equilibrium and nonequilibrium molecular dynamics simulations of heat conduction in uranium oxide and mixed uranium–plutonium oxide

Tatsumi Arima *, Sho Yamasaki, Kazuya Idemitsu, Yaohiro Inagaki

Institute of Environmental Systems, Faculty of Engineering, Kyushu University, 744 Motooka, Fukuoka 819-0395, Japan

ARTICLE INFO

Article history:
Received 15 January 2007
Accepted 19 February 2008

PACS:
28.41.Bm
28.52.Av
44.10.+i
71.15.Pd

ABSTRACT

The thermal conductivity of nuclear fuels such as UO_{2+x} and $(U,Pu)O_{2-x}$ has been calculated by the molecular dynamics (MD) simulation in terms of oxygen stoichiometric parameter x, temperature and Pu content. In the present study, the MD calculations were carried out in both equilibrium (EMD) and nonequilibrium (NEMD) systems. In the EMD simulation, the thermal conductivity was defined as the time-integral of the correlation function of heat fluxes according to the Green–Kubo relationship. Meanwhile, in the homogeneous NEMD, it was given by the ratio of the time-averaged heat flux to the perturbed external force subjected to each particle in the simulated cell. NEMD, as compared with EMD, gave somewhat precise results efficiently. Furthermore, both MD calculations showed that the thermal conductivity of these oxide fuels decreased with increase of temperature and defects, i.e. excess oxygen or vacancy, and was rather insensitive to Pu content for the stoichiometric fuel.

1. Introduction

Uranium oxide and its solid solution with plutonium oxide, i.e. UO_{2+x} and $(U,Pu)O_{2-x}$, have been the most widely used nuclear fuels. The thermal conductivity is one of the most important thermo-physical properties and is dependent on various fuel parameters such as oxygen-to-metal (O/M) ratio, temperature, Pu content, and so on [1,2]. Especially, the deviation from the O/M ratio of 2.0 allows lowering not only of the thermal conductivity but also of melting point. However, it is not so easy to experimentally control the O/M ratio (or oxygen stoichiometry) for these oxide fuels. For the further improvement of the safety of the fuel management, the more systematic study is needed from the point of view of both experimental and theoretical analyses. Therefore, in the present study, the molecular dynamics (MD) simulation has been carried out to evaluate the thermal conductivity in terms of above fuel parameters.

Using the equilibrium molecular dynamics simulation (EMD), we have ever studied the thermal behaviors of uranium oxide, plutonium oxide, mixed uranium–plutonium oxide and stabilized zirconia systems [3–5]. In the previous studies [3–10], the effectiveness of EMD has been verified for the evaluation of physicochemical properties, e.g. thermal expansion, compressibility, specific heat, thermal conductivity. However, it took the more CPU time to obtain the more reliable results especially for the thermal conductivity. Since the thermal conductivity is a transport coefficient, it must be calculated as the time-integral of the auto-correlation function of the heat currents in the thermal equilibrium system by the Green–Kubo relationship, based on the huge volume of the heat current data being accumulated every calculation time step.

Thus, in the present study, the homogeneous nonequilibrium MD (NEMD) proposed by Evans [11] has been carried out in order to overcome the disadvantage of EMD [12,13]. Because this NEMD does not need the comprehensive change for the EMD algorithm. For instance, the periodic condition used in the EMD calculation can be applied also for the homogeneous NEMD. The thermal conductivity calculated by the NEMD is obtained by the linear response of heat flux to the perturbed external force field. In the present study, we verify the effectiveness of homogeneous NEMD simulation for the evaluation of thermal conductivity of nuclear fuels in comparison with the results from EMD simulations and experiments.

2. Homogeneous nonequilibrium molecular dynamics (NEMD) simulation

2.1. Formalization of thermal conductivity in NEMD algorithm

According to the homogeneous NEMD method proposed by Evans [11], dynamics of the particles in the simulated cell are governed by the following equations of motion:

$$\frac{d\vec{q}_i}{dt} = v_i, \tag{1}$$

$$\frac{d\vec{p}_i}{dt} = \vec{F}_i + \overleftrightarrow{D}_i\vec{F}_{ext}(t) - \alpha\vec{p}_i, \tag{2}$$

* Corresponding author. Tel./fax: +81 92 802 3494.
E-mail address: arimatne@mbox.nc.kyushu-u.ac.jp (T. Arima).

0022-3115/$ - see front matter © 2008 Elsevier B.V. All rights reserved.
doi:10.1016/j.jnucmat.2008.02.067

where $\vec{q}_i$ and $\vec{p}_i$ are the generalized coordinate and momentum of ith particle, v_i the velocity, $\vec{F}_i$ the force, $\vec{F}_{ext}$ the perturbed external force coupled with $\overleftrightarrow{D}_i$ the tensor parameter, α the thermostating parameter. Here, $\overleftrightarrow{D}_i$ means the deviation energy of ith particle from average of energy in the N-particle system. When $\vec{F}_{ext} = 0$ and $\alpha = 0$, the system is under the thermal equilibrium condition. Hamiltonian is the internal energy under the adiabatic condition $\alpha = 0$. Its time-derivative is therefore given by

$$\left(\frac{dH}{dt}\right)_{ad} = \vec{F}_{ext}(t)\sum_{i=1}^{N}\frac{\overleftrightarrow{D}_i\cdot\vec{p}_i}{m_i} = \vec{F}_{ext}(t)\cdot\vec{j}_E, \tag{3}$$

where $\vec{j}_E$ is the heat current. In the linear response theory, if the physical observable is the heat current, then the time-averaged heat current can be expressed as Eq. (4) via Eqs. (1)–(3).

$$\langle\vec{j}_E(t)\rangle_t = \frac{\vec{F}_{ext}}{k_BT}\int_0^\infty dt\langle\vec{j}_E(t)\cdot\vec{j}_E(0)\rangle_{eq}, \tag{4}$$

where each particle is perturbed in one direction by time-independent $\vec{F}_{ext}$. On the other hand, in the equilibrium system where the perturbed field is of course zero, the thermal conductivity is given by the Green–Kubo relationship:

$$\kappa = \frac{1}{Vk_BT^2}\int_0^\infty dt\langle\vec{j}_E(t)\cdot\vec{j}_E(0)\rangle_{eq}. \tag{5}$$

As a result, considering Eqs. (4), Eq. (5) is re-written by

$$\kappa = \lim_{F_{ext}\to 0}\lim_{t\to\infty}\frac{\langle\vec{j}_E(t)\rangle}{VTF_{ext}}. \tag{6}$$

Therefore, the thermal conductivity is given as the proportional constant between the time-averaged heat current and the perturbed external force field in the present NEMD. In the above equations, $\vec{j}_E(t)$ is generally written by

$$\vec{j}_E(t) = \sum_{i=1}^{N}\left[\frac{m_iv_i^2}{2} + \frac{1}{2}\sum_{j\neq i}U(r_{ij})\right]\vec{v}_i + \frac{1}{2}\sum_{i=1}^{N}\vec{v}_i\cdot\vec{r}_{ij}\vec{F}_{ij}. \tag{7}$$

This energy current in the Coulomb system was given by Bernu, based on the Ewald method [14]. And $\overleftrightarrow{D}_i$ is redefined using $\overleftrightarrow{D}_i^*$, which $\sum_{i=1}^{N}\vec{v}_i\cdot\overleftrightarrow{D}_i^* = \vec{j}_E(t)$, as

$$\overleftrightarrow{D}_i = \overleftrightarrow{D}_i^* - \frac{1}{N}\sum_{j=1}^{N}\overleftrightarrow{D}_j^*. \tag{8}$$

The detail description of $\overleftrightarrow{D}_i^*$ was given by Motoyama [15]. Also in the present NEMD calculation, D_i defined as Eq. (8) was used in Eq. (2).

2.2. NEMD simulation procedure

In the present study, the NEMD algorithm was incorporated into the MXDORTO program. The original MXDORTO was developed by

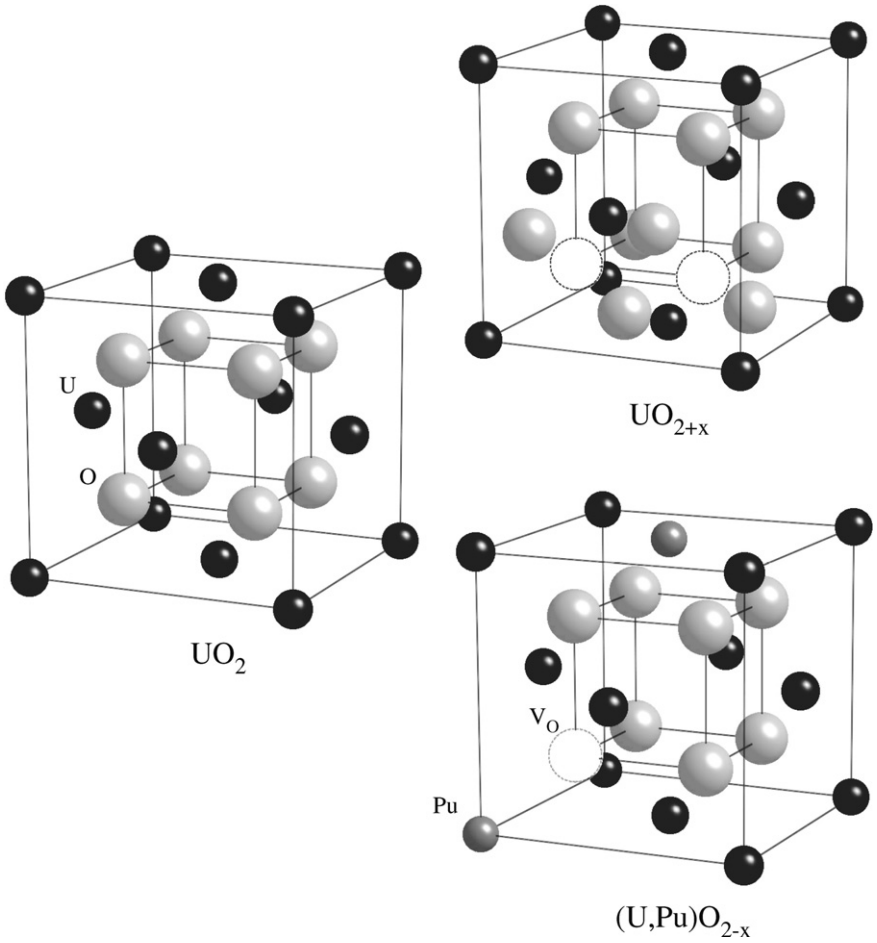

Fig. 1. The crystal structures of UO_2, UO_{2+x} and $(U,Pu)O_{2-x}$. All configurations are based on the fluorite structure. Black balls stand for uranium (U), medium gray for plutonium (Pu), light gray for oxygen (O), white for oxygen vacancy (V_O).

Kawamura for the EMD simulation [16]. In the present calculations, the Born–Mayer–Huggins (BMH) potential with the partially ionic model (PIM) was employed to each ion pair in simulated crystals. This potential function is given by

$$U_{\mathrm{PIM}}(r_{ij}) = \frac{z_i z_j e^2}{r_{ij}} + f_0(b_i + b_j)\exp\left(\frac{a_i + a_j - r_{ij}}{b_i + b_j}\right) - \frac{c_i c_j}{r_{ij}^6}, \quad (9)$$

where z_i is the effective charge of type i ion, e the electron charge, r_{ij} the distance between i and j ions, f_0 the adjustable parameter. Potential parameters, a_i, b_i and c_i, are given to the ion of types i. The first term of the right side of Eq. (9) stands for Coulomb interaction, which extends to a long-range. In order to avoid the divergence of the calculation concerning the long-range term, the Ewald summation algorithm was introduced into MD programs. Other terms stand for short-range interactions: the second one is the repulsive potential between ionic cores; the third one is originated from van der Waals interaction.

The initial supercells for MD calculations were prepared as follows. U^{4+} and O^{2-} ions were arranged at each sub-lattice site of fluorite structure composing of $3 \times 3 \times 3$ unit cells, which is called the basic supercell here. For hyper-stoichiometric UO_{2+x}, (1) one U^{5+} ion was randomly placed on a cation site in the basic supercell; (2) following U^{5+} ion was placed on the nearest neighbor cation site for the firstly placed U^{5+} ion; (3) two other U^{5+} ions were placed around two previously placed U^{5+} ions; (4) two originally placed and two excess O^{2-} ions were arranged around four U^{5+} ions. Such a defect cluster is depicted in Fig. 1 and is called '2:2:2 cluster' [17,18]. By repeating the process from (1) to (4), the 2:2:2 defect clusters were randomly distributed in the initial supercell. However, this configuration of the defect cluster was just an assumption. Because, the lattice structure of the defect cluster observed in UO_{2+x} has been still discussed [19,20]. According to the phase diagram of U–O system [18], UO_{2+x} with $0 < x < 0.25$ decomposes to UO_{2+x} and U_4O_{9-y} at low temperatures, and has a single phase of UO_{2+x} at temperature greater than ~500 K. Therefore, for the present simulation condition such as $x \leqslant 0.09$ and $T \geqslant 900$ K, UO_{2+x} has a single phase. On the other hand, in hypo-stoichiometric $(U,Pu)O_{2-x}$ with fluorite structure, Pu^{4+} and Pu^{3+} ions were randomly distributed on cation sites in the basic supercell while oxygen vacancies were generated on anion sites to keep the electrical neutrality. Such an example of the lattice structure of hypo-stoichiometric $(U,Pu)O_{2-x}$ is shown in Fig. 1.

The MD simulations were performed according to the following procedure. The initial supercell was prepared as described above. Next, the initial relaxation calculation was done for 2×10^4 steps (=40 ps) to equilibrate the simulated system for desired temperature and pressure. Then, for the EMD simulation, the calculations of thermal conductivity were performed 3–5 runs of 5×10^5 time steps in the micro-canonical ensemble (N,V,E). On the other hand, for the NEMD simulation, its calculation was performed $5–10 \times 10^4$ time steps for each direction (x, y or z) under the Nosé thermostat control. In addition, the thermal conductivity was calculated by varying the external force field in the NEMD system. Except for UO_2 case, five different F_{ext} values were applied for many cases (hyper- and hypo-stoichiometric ones) in the NEMD system. Regarding UO_2, so many F_{ext} values were applied to check the relationship between the F_{ext} value and the thermal conductivity. As a result, an amount of total CPU time to calculate a value of thermal conductivity for the NEMD system was less than or equal to that for the EMD system.

2.3. Determination of potential parameters

In order to simulate the hyper-stoichiometric UO_{2+x}, the potential parameter of U^{5+} ion was newly needed. Then, we determined this potential parameter to have the lattice constant from MD fit one from experimental data in the O/M range from 2.02 to 2.09 [21]. Fig. 2(a) and (b) show the lattice parameter and compressibility, respectively [21,22]. For the O/M = 2.00, reliable lattice parameter was measured as a function of temperature [23], and many

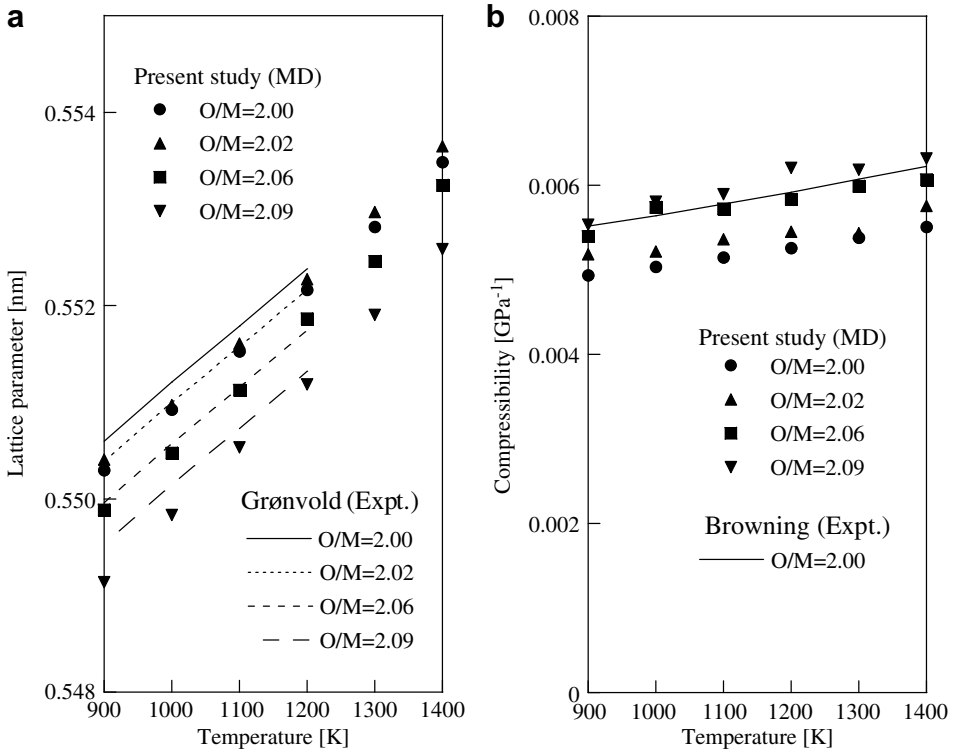

Fig. 2. (a) Relationship between UO_{2+x} lattice parameter and temperature. Experimental data was measured for O/M from 2.00 to 2.09 by Grønvold [21]. (b) Compressibility as a function of temperature. Experimental data of UO_2 at high temperatures was reported by Browning [22].

Table 1
Born–Mayer–Huggins interatomic potential parameters

Ion	z_i	a_i (nm)	b_i (nm)	c_i ($J^{-0.5}$ nm^3 $mol^{-0.5}$)	Source
U^{5+}	3.375	0.1201	0.00303	0.0	Present study
U^{4+}	2.70	0.1318	0.00360	0.0	[3,4]
Pu^{3+}	2.025	0.12217	0.00128	0.0	[4]
Pu^{4+}	2.70	0.1272	0.00325	0.0	[3,4]
O^{2-}	−1.35	0.1847	0.01660	1.294	[26,27]

experimental data of compressibility (=inverse of bulk modulus) were also measured at room temperature [24,25], so that the potential parameter of U^{4+} was optimized using these experimental data. Browning's data seems to be a little higher than the one obtained from MD at $T \geqslant 900$ K. However, Browning's data [22] also seemed to be a little higher than other experimental data at room temperature [24,25]. On the other hand, for hyper-stoichiometric UO_{2+x}, the lattice parameter was measured only by Grønvold [21], and there were no data of compressibility even at room temperature. As a result, there is a contradiction on lattice constant between O/M = 2.00 and 2.02. The ionicity of 67.5% and the potential parameters of O^{2-} ion were obtained from the literature [26,27]. The potential parameters used in the present study are summarized in Table 1.

Fig. 2(a) shows a decrease in lattice parameter of UO_{2+x} by addition of excess oxygens in agreement with experimental data [21]. However, such a result was not discussed on the configuration of the defect cluster. So, pair correlation functions were calculated as well as lattice parameter and compressibility in order to evaluate the potential parameters for the 2:2:2 cluster. Fig. 3 shows pair correlation functions such as O–O, U–O and U–U for UO_2 and UO_{2+x} at 1000 K. Except for U^{5+}–O^{2-}, pair correlation functions of UO_{2+x} diffuse on nominal positions calculated for UO_2. Unfortunately, this result shows that the initial configuration of the 2:2:2 cluster cannot be kept during the calculation for the thermal relaxation. Therefore, the pair potential function with partially ionic charge in this study might be oversimplified to reconstruct the configuration of such a complex defect cluster.

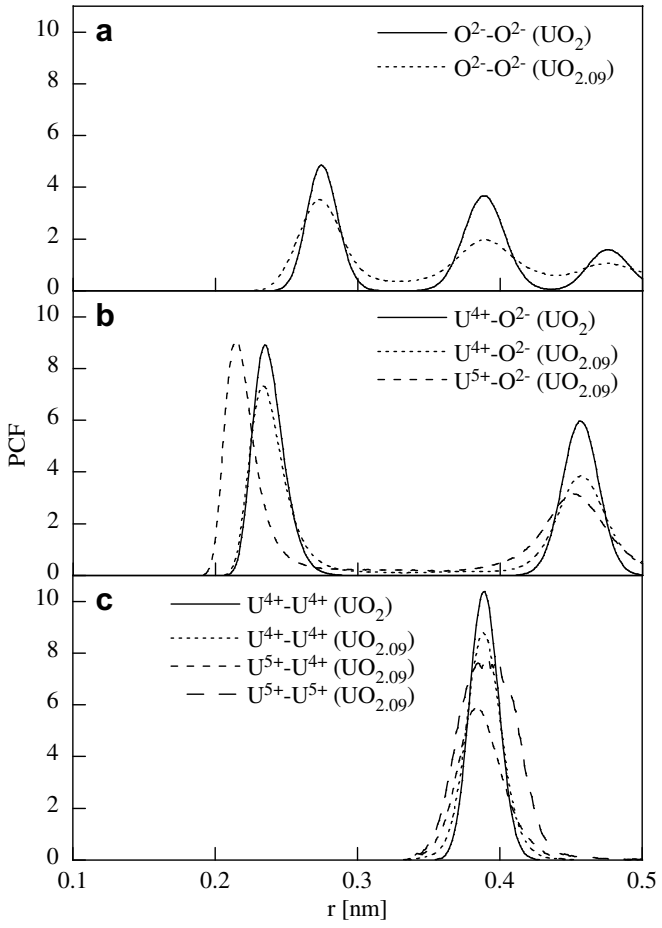

Fig. 3. Pair correlation functions of: (a) O–O, (b) U–O and (c) U–U for UO_2 and $UO_{2.09}$. These results were calculated at 1000 K.

3. Results and discussion

3.1. Perturbed heat flux and oxygen stoichiometric parameter

In the equilibrium system, the thermal conductivity is defined as Eq. (5) based on the Green–Kubo relationship. Our previous study showed that the auto-correlation function of heat currents converged in the shorter time as the oxygen stoichiometric parameter increased [4]. As a result, the thermal conductivity of nonstoichiometric oxide was lower than that of the stoichiometric one. On the other hand, in the nonequilibrium system, the thermal conductivity is directly obtained from the perturbed heat current. Here, the time-averaged heat current divided by V and T is defined as the time-averaged heat flux (see Eq. (6)). Fig. 4 shows the time-averaged heat flux in x-direction at 1000 K as a function of time step. And each figure shows the change of the heat flux after the perturbation onset. It seems that the heat flux approaches to a constant value with increasing the time steps. The thermal conductivity can be obtained as this convergent value divided by F_{ext}. In Fig. 4, it is found that the convergent value for the heat flux of nonstoichiometric oxides decreases regardless of the large F_{ext} value.

3.2. Determination of thermal conductivity for the homogeneous NEMD

Fig. 5(a) shows the time-averaged heat flux as a function of F_{ext} for the UO_2 system. For small F_{ext} values, the heat flux increases linearly with F_{ext} at each temperature. But, it abruptly increases at a certain F_{ext} value, which means the breakdown of the linear response. For such a case, temperature cannot be controlled and increases with time step. Hereafter, this critical value is defined as the maximum F_{ext}. In addition, this figure shows that the maximum F_{ext} value decreases with a decrease of temperature. It means that the perturbed heat flux is very sensitive to F_{ext} value at low temperatures. Furthermore, the temperature of the system is also sensitive to F_{ext} value, which means that the temperature control becomes difficult at low temperatures. Once this maximum F_{ext} can be provided to avoid the nonlinear relationship between the F_{ext} value and the heat flux, the thermal conductivity is determined efficiently and precisely. In principle, it is preferable for the F_{ext} value to be as small as possible for the linear response theory. However, if the F_{ext} value is too small, the effect on perturbed heat flux will be also small. As a result, larger F_{ext} values in the linear response region were required to precisely determine the thermal conductivity. For the UO_2 system, the thermal conductivity is plotted as a function of F_{ext} in Fig. 5(b). In this figure, the variation of thermal conductivity is relatively small at the vicinity of the maximum F_{ext} value. In addition, it is shown that as temperature increases, the thermal conductivity decreases. Fig. 6 shows the maximum F_{ext} value as a function of the thermal conductivity. The relationship in stabilized zirconia system with fluorite structure was given by Yoshiya et al. [28] as follows:

$$\mathrm{Max}.F_{ext} = 10^{M} \times \kappa^{-N}. \quad (11)$$

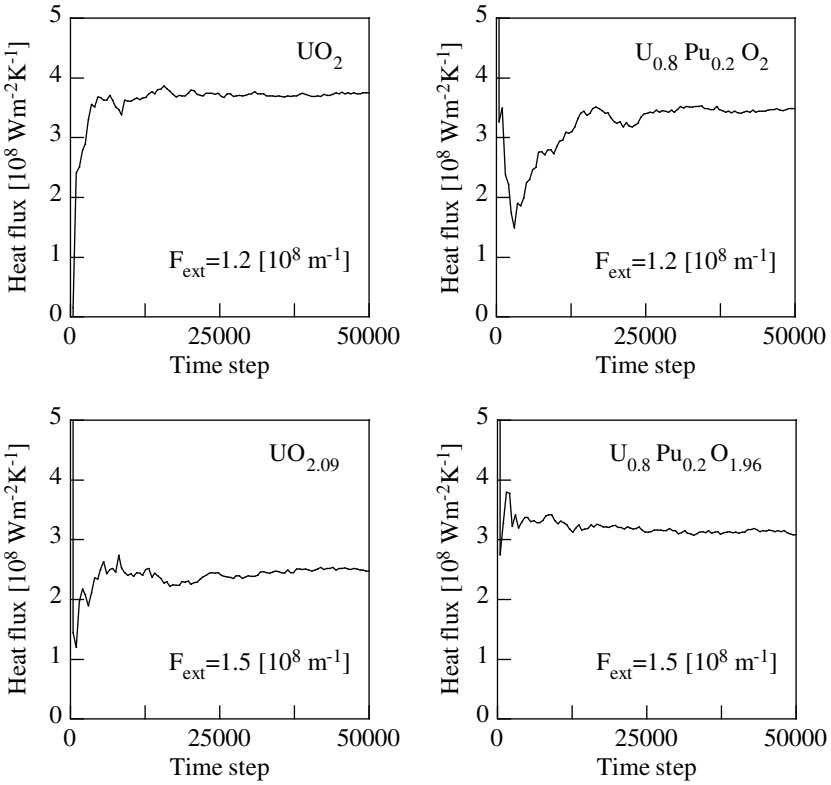

Fig. 4. Time-averaged heat flux calculated by NEMD for various oxides at 1000 K as a function of time step.

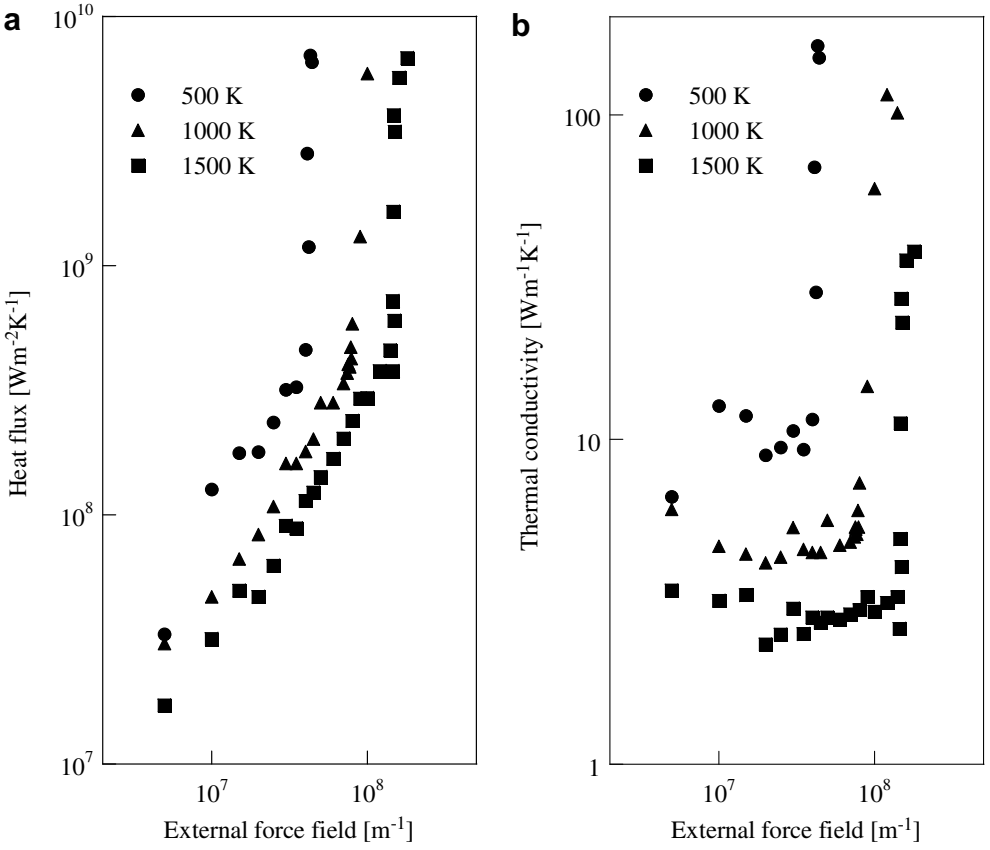

Fig. 5. Time-averaged heat flux (a) and thermal conductivity (b) as a function of F_{ext} for the UO_2 system.

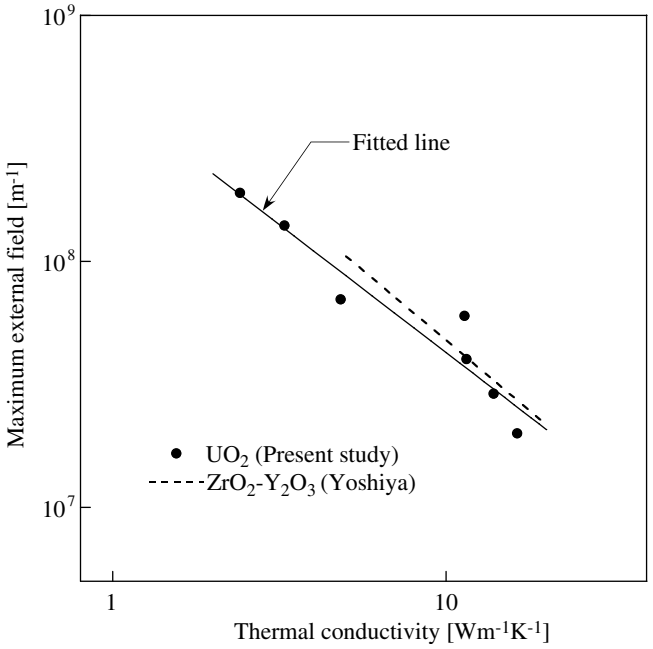

Fig. 6. The maximum F_{ext} value as a function of the thermal conductivity for the UO_2 system. Sold symbols and solid line stand for the result from NEMD and its least square fitting, respectively. Dotted line was obtained for the ZrO_2–Y_2O_3 system [28].

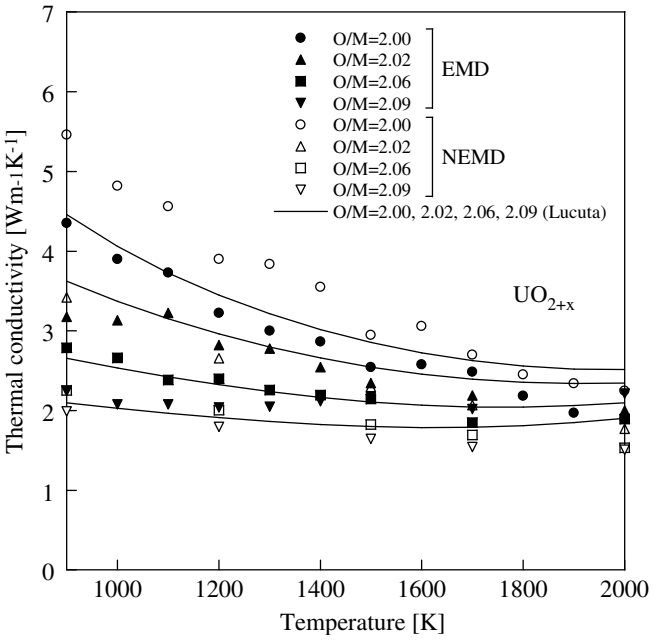

Fig. 7. Thermal conductivity of UO_{2+x} (x = 0, 0.02, 0.06, 0.09) as a function of temperature. Solid symbols stand for EMD, open symbols for NEMD, solid line for Ref. [29].

According to this formula, for zirconia system, M and N were obtained to be 8.82 and 1.14, respectively [28]. For UO_2 system, we obtained M = 8.65 and N = 1.01. As a result, it might not be so different for any fluorite crystal system, and for other materials with fluorite structure, the relationship given by Eq. (11) can provide the guide to set the proper F_{ext} values.

3.3. Thermal conductivities of UO_{2+x} and $U_{0.8}Pu_{0.2}O_{2-x}$ in EMD and NEMD systems

The MD thermal conductivity of UO_{2+x} is plotted as a function of temperature in Fig. 7, together with experimental results [29]. Thermal conductivity of UO_{2+x} decreases with increasing temperature and oxygen stoichiometric parameter x. The experimental thermal conductivity seems to increase slightly at high temperatures since the contribution of conduction electrons becomes large. Of course such a contribution was not considered in MD simulations. The results from MD calculations are originated from the pure phonon conduction. For $x > 0$, excess oxygens scattered the phonons, therefore they caused to the decrease in thermal conductivity. For the stoichiometric UO_2, the thermal conductivity calculated by NEMD is relatively large at low-middle temperatures (<1400 K). Moore et al. showed that the phonons were also scattered by the magnetic moment of U and its contribution was independent on temperature above 80 K [30]. In addition, its contribution was much larger than that from scattering due to grain boundaries. Therefore, the thermal conductivities of single crystal and polycrystalline UO_2 were estimated to be comparable in the wide range of temperature [30]. Considering the contribution of phonon scattering due to magnetic moment of U and unexpected lattice defects (e.g. impurities), the thermal conductivity calculated by EMD seems to be underestimated for the stoichiometric UO_2 at low-middle temperatures in comparison to literature data by Lucuta [29]. Regarding the difference between EMD and NEMD results, these should be equal essentially if the size of supercell is large enough, and if total number of steps to calculate the thermal conductivity is also large. Unfortunately, the information relating these dependences of thermal conductivity cannot be presented here. Especially for the condition where x = 0 and temperature is low, such an effect is serious, so that the EMD thermal conductivity may be underestimated [31]. For UO_2, the thermal conductivities calculated by Eq. (5), which is an integral of autocorrelation function of heat currents, converged extremely slowly with integration time and its fluctuation was estimated to be

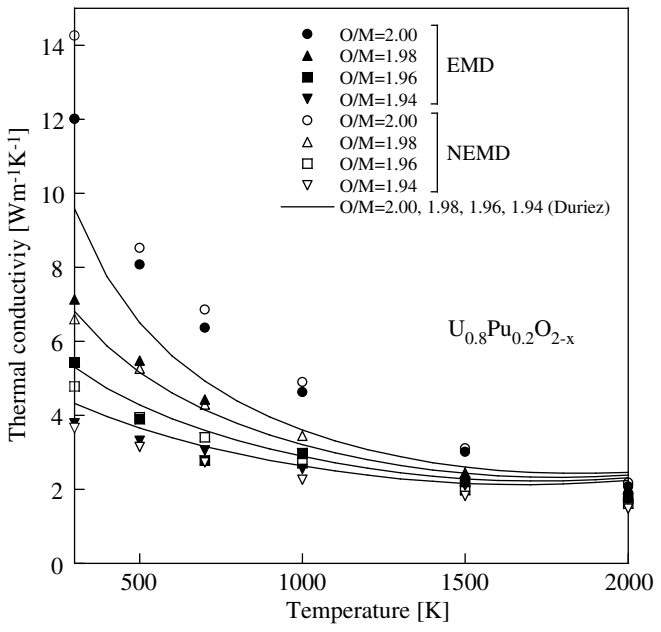

Fig. 8. Thermal conductivity of $U_{0.8}Pu_{0.2}O_{2-x}$ (x = 0, 0.02, 0.04, 0.06) as a function of temperature. Solid symbols stand for EMD, open symbols for NEMD, solid line for Ref. [1].

approximately 30% at $T \leqslant 700$ K. At higher temperatures, the fluctuation was conservatively estimated to be 20–25%.

For hypo-stoichiometric $U_{0.8}Pu_{0.2}O_{2-x}$ in Fig. 8, the thermal conductivity also decreases with increasing temperature and oxygen deficient parameter x. The thermal conductivities are in good agreement among EMD, NEMD and the experiment without for stoichiometric $U_{0.8}Pu_{0.2}O_2$ [1,3]. Both MD simulations gave the larger thermal conductivities than the experiment in low-middle temperatures for stoichiometric $U_{0.8}Pu_{0.2}O_2$. This might be caused from the contribution from phonon scattering due to the magnetic moment of U [30]. The thermal conductivity for $x > 0$ decreases with increase of oxygen deficient parameter because of phonon scattering by oxygen vacancies, which is well reproduced by both EMD and NEMD calculations.

As shown in Figs. 7 and 8, the thermal conductivity calculated by the NEMD system seems to change as a function of temperature with less fluctuations, in comparison with that obtained by EMD. In order to improve the result from EMD simulation, the larger volume of heat current data is required. However, in principle the error of calculation accumulates with number of time steps for the MD simulation, and it is not economical for the CPU cost. On the other hand, the homogeneous NEMD required $5–10 \times 10^4$ of number of time steps for one run compared to that for EMD ($=5 \times 10^5$ time steps). As a result, if appropriate F_{ext} values are chosen for the simulated condition, the thermal conductivity is expected to be determined more precisely and efficiently for the NEMD system.

4. Conclusions

For uranium oxide and its solid solution with plutonium oxide, EMD and NEMD simulations were performed to evaluate the thermal conductivity in terms of temperature, oxygen stoichiometric parameter and Pu content. Both MD calculations show that the thermal conductivity deceases with increase of temperature because of the Umklapp process. Compared stoichiometric UO_2 to $(U,Pu)O_2$, the effect of Pu addition is relatively small. On the other hand, for hyper-stoichiometric UO_{2+x}, the thermal conductivity decreases with increase of x, and for hypo-stoichiometric $(U,Pu)O_{2-x}$, it decreases with increasing x. In these nonstoichiometric oxides, the former is caused by excess oxygens, and the latter by oxygen vacancies. It concludes that the present MD calculations well explain the effect of phonon scattering by Umklapp process and by lattice defects on the thermal conductivity. Compared to the EMD calculation with Green–Kubo relationship, the homogeneous NEMD calculation with the linear response to the perturbed external force gave the thermal conductivity with less fluctuations and with less CPU time as a function of temperature and x. Furthermore, the NEMD calculation is also expected to obtain the more precise result with appropriate F_{ext} values.

Acknowledgments

The authors would like to thank K. Kawamura for usage of the MXDORTO program, and S. Motoyama for advice to calculate the thermal conductivity.

References

[1] C. Duriez, J.P. Alessandri, T. Gervais, Y. Philipponneau, J. Nucl. Mater. 277 (2000) 143.
[2] J.K. Fink, J. Nucl. Mater. 279 (2000) 1.
[3] T. Arima, S. Yamasaki, Y. Inagaki, K. Idemitsu, J. Alloys Comp. 400 (2005) 43.
[4] T. Arima, S. Yamasaki, Y. Inagaki, K. Idemitsu, J. Alloys Comp. 415 (2006) 43.
[5] T. Arima, S. Yamasaki, K. Yamahira, K. Idemitsu, Y. Inagaki, C. Degueldre, J. Nucl. Mater. 352 (2006) 309.
[6] P. Sindzingre, M.J. Gillan, J. Phys.: Condens. Matter. 2 (1990) 7033.
[7] P.J.D. Lindan, M.J. Gillan, J. Phys.: Condens. Matter. 3 (1991) 3929.
[8] K. Yamada, K. Kurosaki, M. Uno, S. Yamanaka, J. Alloys Comp. 307 (2000) 1.
[9] K. Yamada, K. Kurosaki, M. Uno, S. Yamanaka, J. Alloys Comp. 307 (2000) 10.
[10] K. Kurosaki, K. Yamada, M. Uno, S. Yamanaka, K. Yamamoto, T. Namekawa, J. Nucl. Mater. 294 (2001) 160.
[11] D.J. Evans, G.P. Morriss, Statistical Mechanics of Nonequilibrium Liquids, Academic, London, 1990.
[12] C. Pierleoni, G. Ciccotti, B. Bernu, Europhys. Lett. 4 (1987) 1115.
[13] C. Pierleoni, G. Ciccotti, J. Phys.: Condens. Matter. 2 (1990) 1315.
[14] B. Bernu, P. Vieillefosse, Phys. Rev. A 18: (1978) 2345.
[15] S. Motoyama, Y. Ichikawa, Y. Hiwatari, A. Oe, Phys. Rev. B 60 (1999) 292.
[16] K. Hirao, K. Kawamura, Material Design Using Personal Computer, Shokabo, Tokyo, 1994.
[17] B.T.M. Willis, Acta Crystallogr. A34 (1978) 88.
[18] B.T.M. Willis, J. Chemical Society, Faraday Trans. II 83 (1987) 1073.
[19] S.D. Conradson, D. Manara, F. Wastin, D.L. Clark, G.H. Lander, L.A. Morales, J. Rebizant, V.V. Rondinella, Inorg. Chem. 43 (2004) 6922.
[20] F. Garrido, A.C. Hannon, R.M. Ibberson, L. Nowicki, B.T.M. Willis, Inorg. Chem. 45 (2006) 8408.
[21] F. Grønvold, J. Inorg. Nucl. Chem. 1 (1955) 357.
[22] P. Browning, G.J. Hyland, J. Ralph, High Temp. High Press. 15 (1983) 169.
[23] D.G. Martin, J. Nucl. Mater. 152 (1988) 94.
[24] U. Benedict, G.D. Andreetti, J.M. Fournier, A. Waintal, J. Phys. (France) Lett. 43 (1982) L171.
[25] V. Roque, B. Cros, D. Baron, P. Dehaudt, J. Nucl. Mater. 277 (2000) 211.
[26] H. Inaba, R. Sagawa, H. Hayashi, K. Kawamura, Solid State Ionics 122 (1999) 95.
[27] H. Hayashi, R. Sagawa, H. Inaba, K. Kawamura, Solid State Ionics 131 (2000) 281.
[28] M. Yoshiya, A. Harada, M. Takeuchi, K. Matsunaga, H. Matsubara, Mol. Simul. 30 (2004) 953.
[29] P.G. Lucuta, Hj. Matzke, I.J. Hastings, J. Nucl. Mater. 232 (1996) 166.
[30] J.P. Moore, D.L. McElroy, J. Am. Ceram. Soc. 54 (1971) 40.
[31] P.K. Schelling, S.R. Phillpot, P. Keblinski, Phys. Rev. B 65 (2002) 144306-1.